

Lumen Formation Is an Intrinsic Property of Isolated Human Pluripotent Stem Cells

Kenichiro Taniguchi,^{1,*} Yue Shao,⁵ Ryan F. Townshend,¹ Yu-Hwai Tsai,^{1,2} Cynthia J. DeLong,¹ Shawn A. Lopez,¹ Srimonta Gayen,³ Andrew M. Freddo,¹ Deming J. Chue,¹ Dennis J. Thomas,¹ Jason R. Spence,^{1,2} Benjamin Margolis,^{2,4} Sundeep Kalantry,³ Jianping Fu,⁵ K. Sue O'Shea,¹ and Deborah L. Gumucio^{1,*}

¹Department of Cell and Developmental Biology

²Department of Internal Medicine

³Department of Human Genetics

⁴Department of Biological Chemistry

University of Michigan Medical School, Ann Arbor, MI 48109, USA

⁵Department of Mechanical Engineering, University of Michigan, Ann Arbor, MI 48109, USA

*Correspondence: taniguch@med.umich.edu (K.T.), dgumucio@med.umich.edu (D.L.G.)

<http://dx.doi.org/10.1016/j.stemcr.2015.10.015>

This is an open access article under the CC BY-NC-ND license (<http://creativecommons.org/licenses/by-nc-nd/4.0/>).

SUMMARY

We demonstrate that dissociated human pluripotent stem cells (PSCs) are intrinsically programmed to form lumens. PSCs form two-cell cysts with a shared apical domain within 20 hr of plating; these cysts collapse to form monolayers after 5 days. Expression of pluripotency markers is maintained throughout this time. In two-cell cysts, an apical domain, marked by EZRIN and atypical PKC ζ , is surrounded by apically targeted organelles (early endosomes and Golgi). Molecularly, actin polymerization, regulated by ARP2/3 and mammalian diaphanous-related formin 1 (MDIA), promotes lumen formation, whereas actin contraction, mediated by MYOSIN-II, inhibits this process. Finally, we show that luminal shape can be manipulated in bioengineered micro-wells. Since lumen formation is an indispensable step in early mammalian development, this system can provide a powerful model for investigation of this process in a controlled environment. Overall, our data establish that lumenogenesis is a fundamental cell biological property of human PSCs.

INTRODUCTION

Proper development of many tissues and organs (e.g., gut, kidney, blood vessels, lung, etc.) requires the formation of luminal structures of various shapes (Shao et al., 2015). Indeed, one of the first behaviors of early embryonic epiblast cells is formation of the lumen of the proamniotic cavity (Luckett, 1975; Rossant and Tam, 2009). This process is still poorly understood but is essential for the further successful development of the embryo. In vitro, many stem cells grow into organoids with luminal structures (Lancaster and Knoblich, 2014), indicating that self-organization to form lumens is intrinsic to a variety of stem cell types. Because proper morphogenesis and function are so dependent on luminal integrity in many settings, a detailed understanding of the lumen-forming process and the mechanisms underlying it is critical for the proper engineering of transplantable tissues.

Much of what we currently know about lumen formation comes from the study of transformed, tissue-specific cell lines such as Madin-Darby canine kidney type 2 (MDCK.2) and Caco-2 (human colorectal cancer) cells; these cells form polarized luminal cysts de novo when embedded in extracellular matrix (ECM) complex (Martin-Belmonte and Mostov, 2008; Rodriguez-Boulán and Macara, 2014). Using these models, it has been demonstrated that lumen formation is initiated during the first

cell division by the trafficking of apical proteins such as Ezrin, Podocalyxin, and Crumbs3 from the cell periphery to the nascent cytokinetic plane (Bryant et al., 2014; Schlüter et al., 2009). This process allows the establishment of the apical membrane initiation site (AMIS), an actin-rich region that matures to become the lumen (Martin-Belmonte and Mostov, 2008; Rodriguez-Boulán and Macara, 2014). Although MDCK.2 and Caco-2 are useful to model lumen formation in differentiated models (kidney and gut), effective general tools to model development of early embryonic tissues that undergo de novo lumen formation are currently lacking.

We have discovered that when dissociated human embryonic stem cells (hESCs) or human induced pluripotent stem cells (hiPSCs) are plated at low density in 2D or 3D conditions, the first mitotic event frequently generates a two-cell cyst with an AMIS-like domain that matures to a lumen. The lumen-forming capacity of pluripotent stem cells (PSCs) is amenable to manipulation to generate lumens of complex shapes using micro-engineered substrates. Molecularly, we find that, as in MDCK.2 cells, augmenting ROCK (Rho-associated kinase)-MYOSIN-II signaling, which leads to the formation of actin stress fibers (Burrige and Wennerberg, 2004), inhibits apical lumen formation in PSC (Rodríguez-Fraticelli and Martín-Belmonte, 2013). Additionally, we demonstrate a critical role for two separate

actin polymerization processes (via mammalian diaphanous-related formin 1 [MDIA] and via ARP2/3) in lumenogenesis. Overall, our data establish PSCs as effective non-transformed and undifferentiated cells to be identified as a robust model for lumenogenesis.

RESULTS AND DISCUSSION

hESCs Form Polarized Luminal Cysts in 3D Culture

Human embryos undergo lumen formation to generate an amniotic cavity, but this process has not been well studied. Since [Bedzhov and Zernicka-Goetz \(2014\)](#) recently showed that murine ESC can form cysts with dominant lumens by 36–48 hr in a 3D culture system, we tested whether H9 hESC (NIH code, WA09) can also undergo lumenogenesis. H9 cells were grown in standard medium containing Y-27632 (ROCK inhibitor) to inhibit apoptosis ([Ohgushi et al., 2010](#)). Three days after plating dispersed H9 hESC in Geltrex, the vast majority of cells had formed multi-cell cysts, $86.7\% \pm 1.8\%$ of which had a single dominant lumen ([Figure 1A](#)). Similar to MDCK.2 cysts ([Martin-Belmonte and Mostov, 2008](#); [Rodriguez-Boulan and Macara, 2014](#)), hESC cyst lumens are characterized by abundant F-actin and EZRIN (an apical actin binding protein) and are surrounded by apically targeted organelles, including early endosomes (RAB11) and Golgi (GM130) ([Figures 1B–1E](#), individual channels in [Figures S1A–S1D](#)).

A 2D Culture Environment Is Sufficient to Generate hESC-Derived Luminal Cysts; Cells Maintain Pluripotency during Cyst Growth

We next tested whether singly dissociated H9 cells grown in 2D conditions on plates thinly coated with ECM such as Geltrex (required for hESC attachment in feeder-free culture; [Ludwig et al., 2006](#)), can form lumens. Indeed, two cell cysts have a shared EZRIN-rich domain and cystic structures with EZRIN-rich lumens are seen by day 3 ([Figures 1F and 1G](#)). Alternative ECM substrates (e.g., Matrigel or vitronectin) support luminal cyst formation at a frequency similar to Geltrex in 2D culture ([Figures 1H, S1E, and S1F](#)). In contrast, MDCK.2 cells plated on Geltrex in 2D conditions exhibit multiple small regions enriched in aPKC and Ezrin, but dominant central lumens are not observed ([Figure S1G](#)).

Given this previously uncharacterized behavior of hESCs, we further explored pluripotency status over time during lumen formation in 2D conditions. At 20 hr, $63.5\% \pm 7.7\%$ of two-cell clones have EZRIN-rich AMIS regions, and at 3 days, $79.0\% \pm 1.3\%$ are lumenally polarized, with significantly larger EZRIN-rich areas ([Figures 1H and S1H](#)). By day 5, the lumen-like structure of hESC cysts collapses and the cells form monolayers ([Figures 1F and](#)

[1G, 5 days](#)); all but the most peripheral cells are EZRIN positive, potentially due to compaction and epithelialization. Importantly, nuclear expression of the pluripotency markers, NANOG and POU5F1 persists throughout this time course ([Figures 1F and 1G](#)). With further growth of the monolayer colonies, the outer layer of EZRIN-free cells disappears, but expression of pluripotency markers persists ([Figures 1F and 1G, monolayer](#)). At the RNA level, *POU5F1*, *NANOG*, and *SOX2* are expressed at similar levels in luminal cysts and monolayer culture ([Figure S1I](#)).

Luminal Shape Can Be Manipulated

Since hESC cysts collapse by 5 days in 2D culture, we tested whether lumens can be maintained if the cells are cultured with an ECM overlay. Indeed, when cells were overlaid with 2% Geltrex, lumens persisted at 5 days ([Figures 2A and 2B](#)). These lumens were relatively flat, limited by the height of the Geltrex overlay ([Figure 2Ai](#)). To determine the extent to which luminal shape can be physically influenced, we plated dissociated H9 cells in manufactured micro-wells, troughs, or wide channels of various shape, in the presence of an ECM overlay. In circular wells 30 μm in diameter and 30 μm deep, lumens are tall and barrel shaped after 5 days ([Figures 2C and S1J](#)). In long micro-trenches (30 μm wide \times 30 μm deep), elongated tubes are seen ([Figure 2D](#)). Finally, complex and branched luminal shapes can be produced in larger channels (200 μm wide \times 300 μm deep). The lumen in such tubes is continuous, as demonstrated by EZRIN staining ([Figure 2E](#)). Importantly, these cells maintain POU5F1 expression, demonstrating that pluripotent cells can be guided by external cues to form luminal tubes of a variety of configurations. This engineered system provides a robust model of lumen formation, allowing the generation of lumens of malleable shape, under well-controlled conditions that could be valuable for the study of a variety of biological activities, such as boundary formation, shear flow, or morphogen gradient behavior.

hESCs Form a Highly Organized AMIS by the Two-Cell Stage

In 3D conditions, two-cell clones of MDCK.2 cells form an AMIS that is enriched in apical markers ([Figure S2A](#)) ([Rodriguez-Boulan and Macara, 2014](#)). To establish whether the EZRIN-rich structure in two-cell hESC cysts has characteristics of an AMIS, we grew singly dissociated hESC in a 2D environment. Indeed, at 20 hr, a centrally located actin-rich domain that colocalizes with apical proteins, including EZRIN and aPKC, is present ([Figures 3A and 3B](#), individual channels in [Figures S2B–S2I](#)). Surrounding these apical proteins is a domain that is enriched in GM130, RAB11, and the tight junction marker ZO-1 ([Figures 3C–3E](#)). Centrosomes (γ -TUBULIN) are adjacent to the apical domain ([Figure 3F](#)), as previously noted for the MDCK.2

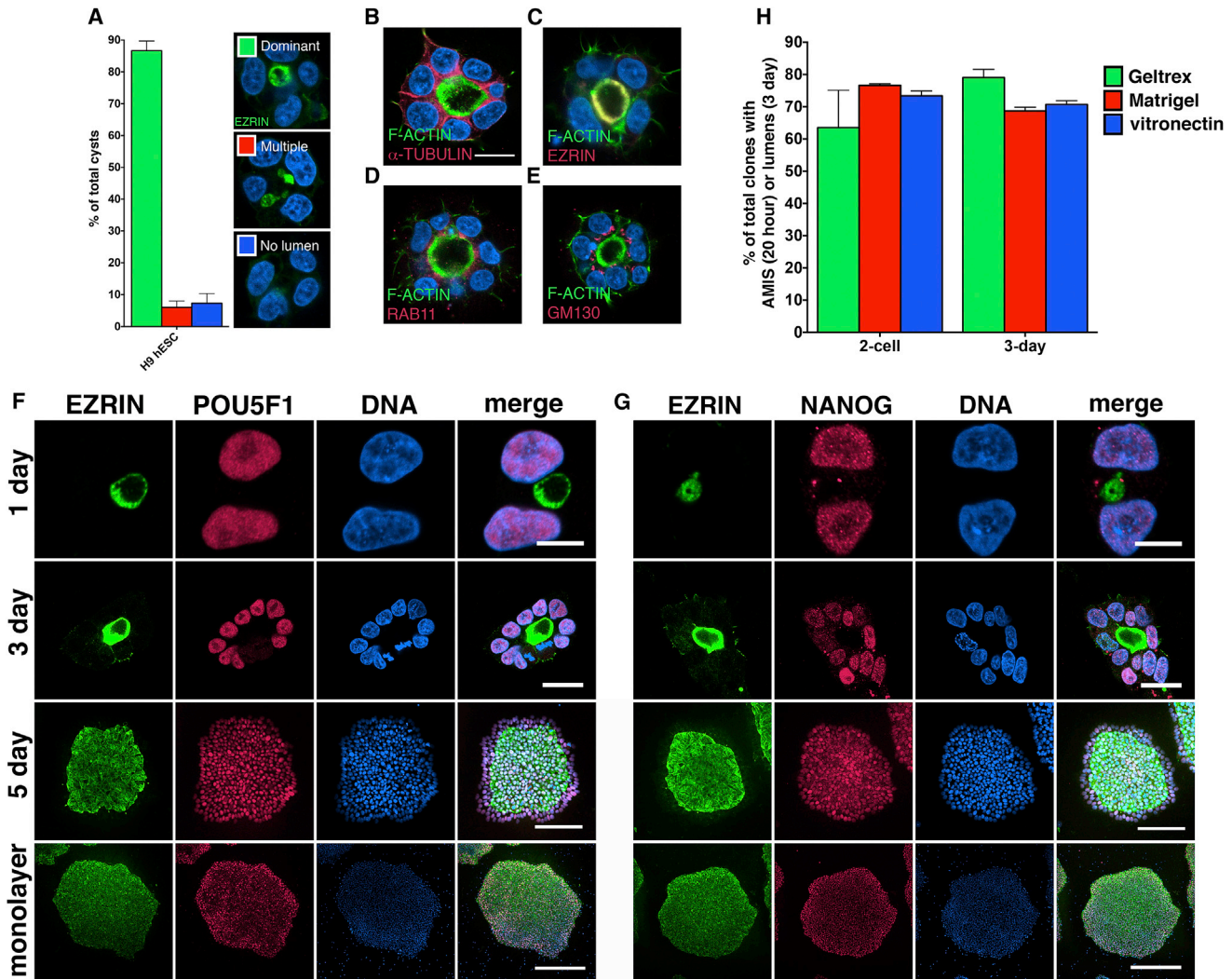
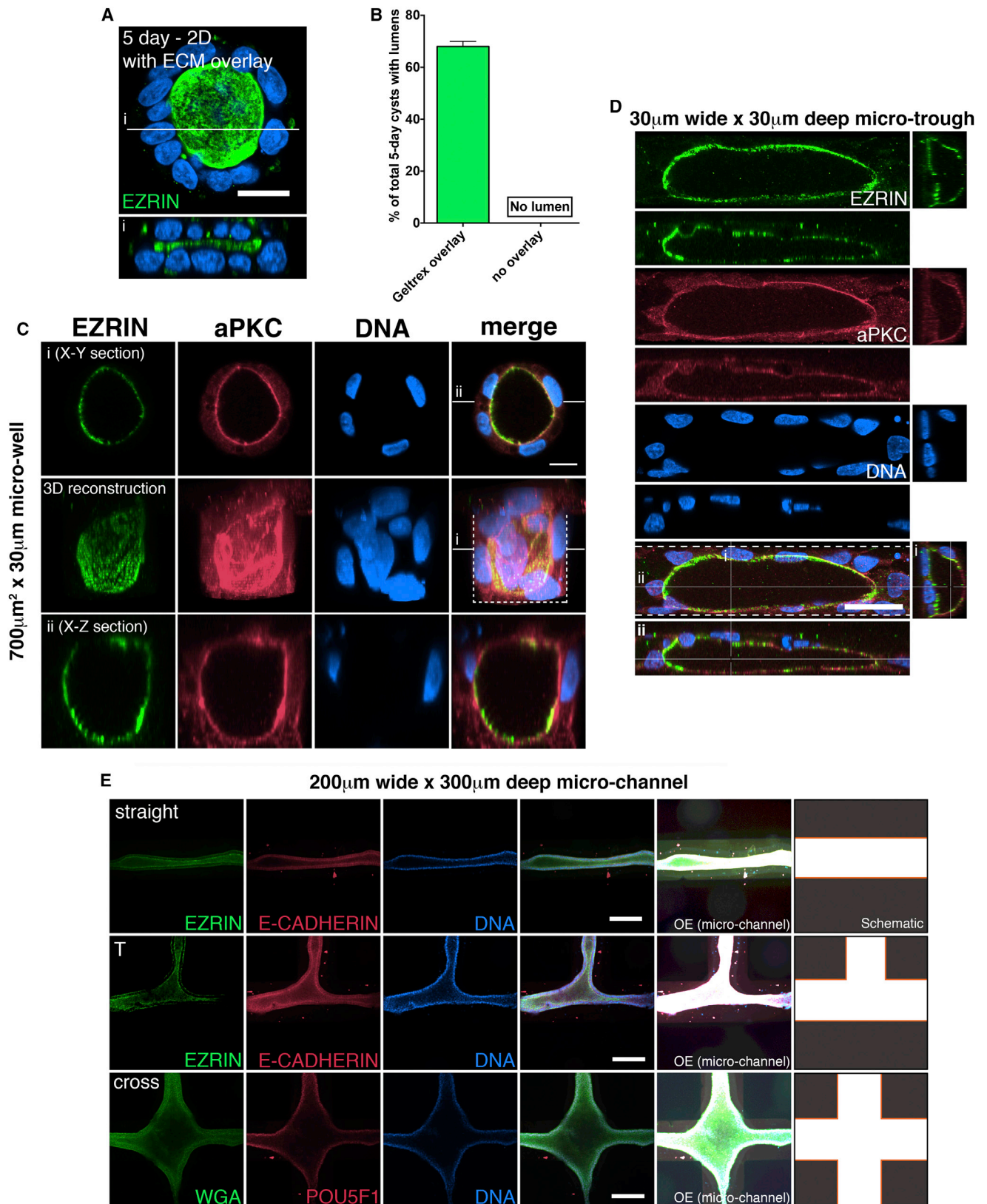


Figure 1. hESCs Undergo Cyst Formation while Maintaining Pluripotency Marker Expression

(A) Quantitation of H9 hESC cyst phenotypes in a 3D culture system grown for 3 days. Images at right show three distinct phenotypes of H9 cysts (EZRIN immunostaining, green): cysts containing a single lumen are categorized as “dominant” (green bar); cysts with multiple lumens are called “multiple” (red bar), and cysts without clear apical EZRIN accumulation are categorized as “no lumen” (blue bar). Fifty multi-cell clones were counted per independent replicate (total of 150 clones in three experiments). Mean values with SD are plotted. (B–E) Cysts were grown in 3D culture for 3 days; phalloidin (green) stains F-ACTIN. (B) α -TUBULIN immunostaining (red) shows microtubule localization. (C) EZRIN immunostaining (red) overlaps with F-ACTIN (green) and identifies the apical lumen (yellow). (D and E) RAB11 and GM130 immunostaining (red) reveal the localization of early endosomes and Golgi apparatus, respectively. (F and G) Cells plated in 2D conditions were harvested at the indicated stages and stained for an apical marker (EZRIN, green) and pluripotency markers (POU5F1, F, or NANOG, G; red). POU5F1 and NANOG staining is maintained throughout these stages. (H) Quantitation for the frequency of lumen forming two-cell and 3-day clones on different feeder-free substrates, Geltrex (green), Matrigel (red), and vitronectin (blue). The mean value of each independent sample (triplicate samples include at least 50 individual two-cell or multi-cell clones) with SD is plotted per condition. For all images, blue indicates DNA staining (DAPI). Scale bar represents 10 μ m for (B)–(E); 10 μ m for 1 day, 30 μ m for 3 day, 150 μ m for 5 day, and 200 μ m for monolayer in (F) and (G). See also [Figures S1, S3, and S4](#).

AMIS ([Rodríguez-Fraticelli and Martín-Belmonte, 2013](#)), while lateral proteins, E-CADHERIN and β -CATENIN, surround the lumen and line the intercellular junction ([Figures 3G and 3H](#)).

Interestingly, 3D reconstructions of stained cysts reveal that the AMIS of H9 cells is highly organized. Adherens junctions (E-CADHERIN, [Figure 3I](#)) and tight junctions (ZO-1, [Figure 3J](#)) form a well-demarcated ring around the



(legend on next page)



apical region, indicating a high degree of polarization at this very early stage of cyst formation.

Lumen Formation Is Not Limited to H9 Cells and Feeder-Free Conditions

To determine whether lumen formation is a more general property of PSCs, we tested several distinct human ESC lines (NIH code WA01 [H1], WA07 [H7], UM63-1, and UC06 [HSF-6] cells) a human iPSC line (1196a cells) (Chen et al., 2014), a mouse ESC line (E14Tg2a.4 cells) (Hooper et al., 1987), and a mouse epiblast stem cell line (mEpiSC, 22M cells) (Gayen et al., 2015). All tested hESCs and hiPSCs formed lumens by 3 days in 2D Geltrex-coated, feeder-free culture conditions (Figures S3A–S3D), indicating that lumenogenesis is a shared property of multiple types of human PSCs. However, slight differences in the size of the lumen and the frequency of lumen formation were noted (Figures S3C and S3D). Importantly, several of these lines were karyotyped as 3-day cysts and found to be normal (Figures S3E–S3G).

We also compared hESCs (H9, H1, H7, and HSF-6) that had been consistently grown on mouse embryonic fibroblast feeders (MEFs) with feeder-free derivatives of the same lines (Figures S4A–S4E). All lines formed AMIS structures by the two-cell stage at reduced frequency when plated on MEF, with the exception of H7 cells (Figure S4E). With further growth, dominant lumen formation was significantly reduced for all lines, particularly for H1, H7, and HSF-6 cells, revealing line-specific differences in lumen-forming potential, especially in the presence of feeders (Figure S4E, see legend for detailed description).

Bedzhov and Zernicka-Goetz (2014) showed that mouse ESCs form lumens by 36–48 hr in 3D culture. Analysis of the time course of mESC lumen formation reveals an AMIS structure that expands (Figures S4F and S4G, see legend for detailed description). Mouse EpiSCs undergo lumenogenesis as well (Figures S4H and S4I). Interestingly,

AMIS structures in mEpiSCs are 10-fold larger than those seen in mESCs ($0.26 \pm 0.04 \mu\text{m}^2$ in mESCs versus $2.68 \pm 0.33 \mu\text{m}^2$ in mEpiSCs; Figure S4J). Additionally, the AMIS in two-cell H9 cells was >8-fold larger than mEpiSCs ($22.78 \pm 2.48 \mu\text{m}^2$, see two-cell in Figure S1H). This is of interest because mEpiSCs are thought to represent a slightly later stage of development than mESCs. Indeed, mEpiSCs are epigenetically more similar to hESCs than are mESCs (Tesar et al., 2007). Taken together, these results demonstrate that multiple types of human and mouse PSCs are intrinsically programmed to form lumens and that the epigenetic state may affect the lumen-forming characteristics of PSCs, at least in mice.

Role of Actin Cytoskeletal Signaling during hESC Lumenogenesis

In Madin-Darby canine kidney (MDCK) cells, inhibition of ROCK increases lumen formation (Rodríguez-Fraticelli and Martín-Belmonte, 2013). To examine this in hESCs, we treated singly dissociated H9 cells with graded concentrations of the ROCK inhibitor, Y-27632, for 20 hr immediately after seeding. Quantification of AMIS formation in two-cell clones stained for EZRIN shows that increasing levels of ROCK inhibition enhances the frequency of AMIS formation (Figures 4A and 4B). Importantly, in the absence of ROCK inhibition (labeled “DMSO only” in Figure 4), cells die, as previously shown; thus, standard culture conditions often include $10 \mu\text{M}$ Y-27632 for the first 24–48 hr (Ohgushi et al., 2010).

MYOSIN-II activation is downstream from ROCK, and we found that blebbistatin (Figure 4B), a potent inhibitor of MYOSIN-II activity (Straight et al., 2003), also increases AMIS formation. Indeed, MYOSIN-II inhibition promotes more efficient AMIS formation than ROCK inhibition at all tested concentrations (Figure 4B). Together, these data suggest that actin contraction downstream of ROCK-MYOSIN-II inhibits lumen formation in hESCs.

Figure 2. Modulation of Luminal Shape Using Engineered Substrates

(A) Cells plated in 2D conditions for 5 days, treated with mTeSR1 media containing 2% Geltrex for the first 24 hr (ECM overlay) after plating. Media was changed daily using mTeSR1 without Geltrex for 3 more days, and cells were harvested and stained for EZRIN (green). (i) An optical cross section of the cyst is shown in (A); the white line indicates the plane of section.

(B) Frequency of 50 5-day cysts with lumens, as in (A), in the presence or absence of a Geltrex overlay. Mean values with SD are plotted. (C and D) Cells grown for 5 days with ECM overlay in circular micro-wells (C) or long $30 \mu\text{m}$ wide micro-troughs (D) were stained for EZRIN (green) and aPKC (red). Substrates in (C) and (D) are precoated with a thin layer of Geltrex. In (C), a 3D reconstructed image is shown as well as the image of the optical X-Y (i) and X-Z (ii) sections of the imaged cyst. White lines indicate the planes of section. In (D), optical Y-Z (i) and X-Z (ii) sections of the micro-tubes are shown. The planes of section are indicated by white lines. White dotted lines indicate the boundary of the circular micro-well (C) and trough (D).

(E) Cells were plated at high density with ECM overlay in $200 \mu\text{m}$ wide micro-channels of various shapes (pre-coated with a thin layer of Geltrex). After 5 days, cells were stained for EZRIN or WGA, wheat germ agglutinin, (green), and E-CADHERIN or POU5F1 (red). For clarification of the shapes of the channels, overexposed images and schematics are also shown. For all images, blue indicates DNA staining (DAPI).

Scale bars represent $30 \mu\text{m}$ in (A), $10 \mu\text{m}$ in (C), $30 \mu\text{m}$ in (D), and $200 \mu\text{m}$ in (E). See also Figures S1, S3, and S4.

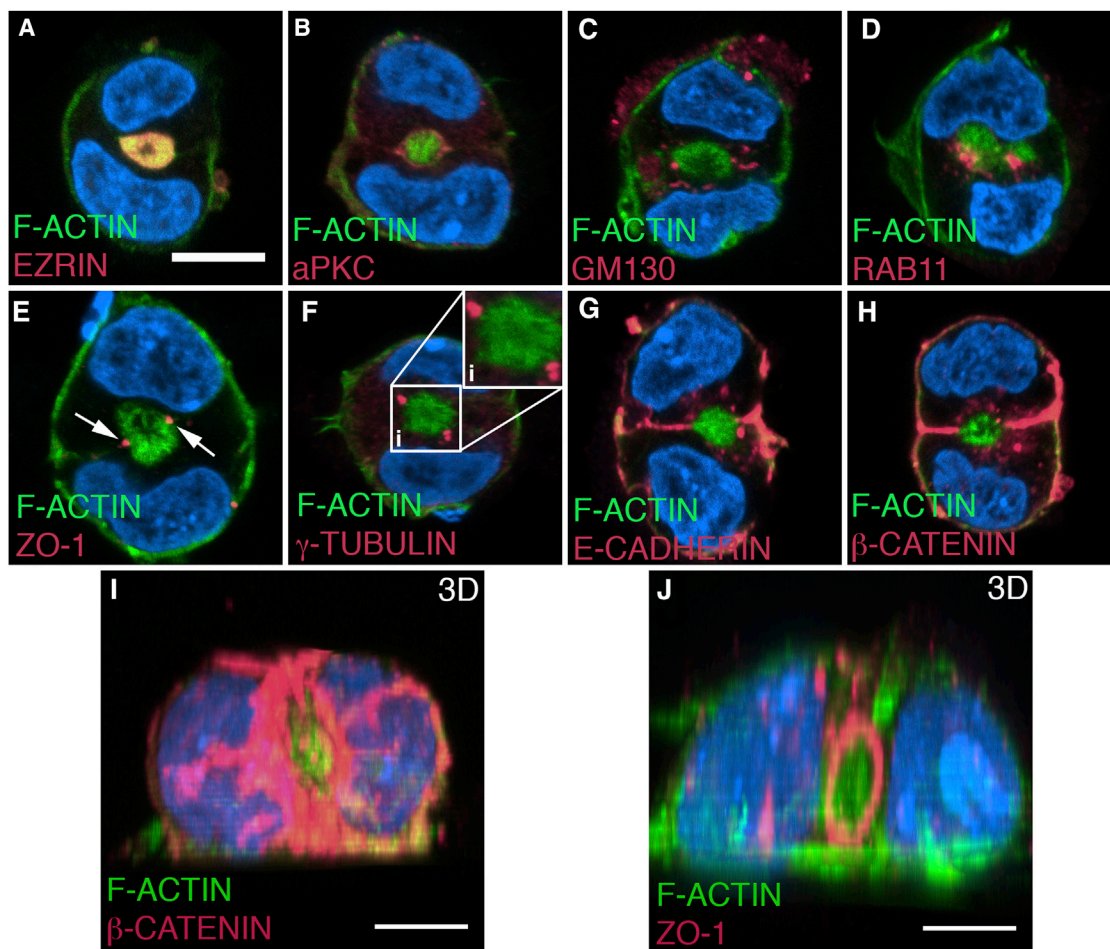


Figure 3. AMIS Formation during hESC Lumenogenesis

(A–H) An F-ACTIN-rich apical domain (green) marks the AMIS. Apically targeted cellular components (EZRIN, A, and aPKC, B, red) are associated with the forming lumen. Markers for apically targeted cellular components (red) surround the AMIS, including Golgi (GM130, C) the early endosome (RAB11, D), and tight junctions (ZO-1, E, arrows indicate the expression domains of ZO-1). Centrosomes, marked by γ -TUBULIN (F, red), lie close to the AMIS. (i) The AMIS in (F) was magnified further (inset) to clarify the organization of centrosomes. E-CADHERIN (G, red) and β -CATENIN (H, red) are associated with the cytokinetic plane and surround the nascent lumen. (I and J) 3D reconstructions of the β -CATENIN (I) and ZO-1 (J) stained cysts for which single sections are shown in (G) and (E), respectively. Both reconstructions are viewed tangentially to the cytokinetic plane to show the zone of β -CATENIN staining surrounding the lumen (I) and the complete ZO1 ring (J).

Scale bars represent 10 μ m for (A)–(J). See also [Figures S2–S4](#).

Actin cytoskeletal organization is also aided by actin polymerization. Formins, which promote the assembly of straight actin filaments, can be inhibited using a small-molecule inhibitor (SMIFH2) that binds to the FH2 or actin-binding domain of the formin proteins (Rizvi et al., 2009). When H9 cells are treated with graded concentrations of SMIFH2, both lumen formation, as well as luminal size, progressively decreases, indicating that formin activity has a positive effect on lumen formation in H9 cells (Figures 4A, 4C, and 4D).

To genetically test the influence of formin activity on lumenogenesis, we transfected H9 cells with GFP-fusion

constructs encoding full-length or a Δ N3 (543–1,192 amino acid) constitutively active mutant form of human MDIA1, a diaphanous-related formin (Sakamoto et al., 2012). Following transfection, sparsely plated cells were harvested at 20 hr, stained for EZRIN, and quantified for lumen formation in GFP-expressing cells. Indeed, H9 cells expressing the MDIA1- Δ N3-GFP construct show a significant increase in lumen formation compared with cells expressing a GFP control plasmid or MDIA1-full-length-GFP, indicating that MDIA activity promotes lumenogenesis (Figures 4E and 4F). Thus, we demonstrate that lumen initiation in hESCs is positively regulated by the RHO-MDIA signaling

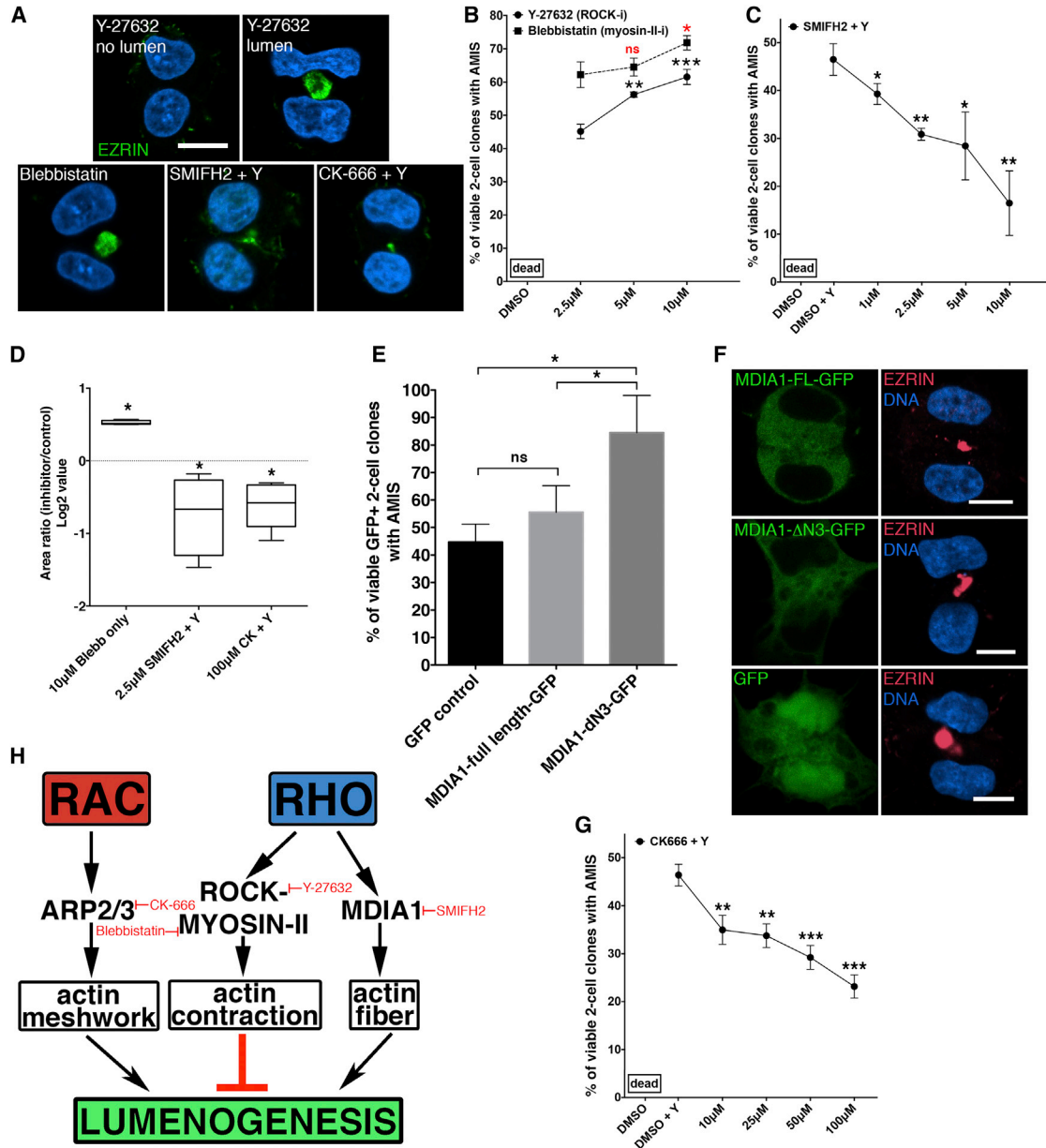


Figure 4. Actin Polymerization Promotes hESC Lumenogenesis

(A) Confocal images of H9 hESCs grown in 2D culture conditions for 20 hr with various inhibitors and immunostained for EZRIN. Two distinct phenotypes are seen in the presence of 10 μ M for Y-27632: clones without a central EZRIN accumulation (no lumen) and clones with EZRIN accumulation at the AMIS (lumen). Cells treated with blebbistatin exhibit lumens, but treatment with SMIFH2 (+10 μ M Y) or CK-666 (+10 μ M Y) reduces lumen size.

(B) Comparison of AMIS formation in hESCs at the two-cell stage in the presence of graded concentrations of Y-27632 (ROCK inhibitor) or blebbistatin (MYOSIN-II inhibitor). Statistical differences are indicated in black for Y-27632 and in red for blebbistatin. Consistent with recent studies, blebbistatin treatment alone rescues dissociation-mediated cell death (Ohgushi et al., 2010).

(C) hESCs were treated with graded concentrations of the formin inhibitor, SMIFH2. Quantitation of AMIS formation at the two-cell stage is shown. Y-27632 was added to hESC cultures to prevent cell death.

(D) Quantitation of the size (area) of the Ezrin⁺ AMIS in H9 clones treated with the indicated small molecules. For each quantitation, four independent sets of 15 individual two-cell clones, treated with the indicated small molecules or experimental control (treated only with Y-27632), were imaged. Images of individual clones, focused at the plane with the largest lumen, were analyzed in ImageJ to determine the surface area of the AMIS. Average of log₂ of normalized value (surface area of small-molecule-treated clones divided by surface area of

(legend continued on next page)



pathway. Previous studies indicated a role for the inverted formin INF2 in lumen organization in MDCK cells (Madrid et al., 2010), suggesting the potential for broad involvement of formins in lumenogenesis.

We next examined the role of branched actin polymerization via ARP2/3, a downstream effector of Rac1-Wiskott-Aldrich syndrome protein (WASP)-WASP-family verprolin-homologous protein (WAVE) complex signaling (Burridge and Wennerberg, 2004). Treatment of H9 cells with CK-666, a small-molecule inhibitor of ARP2/3 (Nolen et al., 2009), resulted in a significant decrease in AMIS formation (Figure 4G). Additionally, resulting lumens were smaller in size (Figures 4A and 4D), suggesting that ARP2/3-induced actin branching is critical for AMIS formation. Together, these data reveal that actin polymerization by both the formin and ARP2/3 pathways is important for lumen establishment in hESCs.

Overall, our data establish that lumenogenesis is a basic cell biological property of a variety of PSCs. At the two-cell stage, PSC cysts contain an AMIS that closely resembles the structure previously described in MDCK cells, though the formation of this structure differs somewhat in human versus mouse cells and may be dependent on the epigenetic state of the cells. It will be of interest to test the lumen-forming potential of recently derived “naive” hESCs (Chan et al., 2013) that are more epigenetically close to ICM-like mESCs, as well as the recently described “region-selective” PSCs, a pluripotent state that appears to be more developmentally advanced than the “primed” state (Wu et al., 2015). The robustness and stereotypical nature of the lumen forming process that we describe in human PSCs makes these cells an excellent model system for the further molecular dissection of the lumenogenesis process. Indeed, our studies have already revealed new aspects of the role of actin polymerization in lumen formation. Furthermore, the malleable nature of the luminal shape, coupled

with the pluripotent characteristics of the cells, will facilitate a wide variety of biological and biomechanical investigations in the context of tube formation and function.

EXPERIMENTAL PROCEDURES

Cell Lines Used in This Study

Several human and mouse PSC lines were used in this study, as were MDCK.2 dog kidney cells (the latter were obtained from ATCC). Human PSCs used in this work included H9 (WA09), H1 (WA01), H7 (WA07), HSF-6 (UC06), and UM63-1. The human iPSC line 1196a was also tested. All protocols for the use of the human PSC lines were approved by the Human Pluripotent Stem Cell Research Oversight Committee at the University of Michigan.

SUPPLEMENTAL INFORMATION

Supplemental Information includes Supplemental Experimental Procedures and four figures and can be found with this article online at <http://dx.doi.org/10.1016/j.stemcr.2015.10.015>.

AUTHOR CONTRIBUTIONS

K.T., R.F.T., Y.S., C.J.D., A.M.F., D.J.C., S.A.L. and D.J.T. performed cyst formation assays. K.T., Y.S., Y.T., and J.R.S. performed experiments using hESCs. C.J.D. and K.S.O. developed the 1196a hiPSC line. Y.S. and J.F. developed microfabrication assay systems. K.T. and B.M. developed the cyst assay protocols. S.G. and S.K. developed the 22M mouse EpiSC line. K.T. and D.L.G. analyzed data, designed experiments, and wrote the manuscript. All other authors edited the manuscript.

ACKNOWLEDGMENTS

We thank the University of Michigan Pluripotent Stem Cell Core and Microscopy and Image Analysis Core and Transgenic Animal Model Core for technical assistance and E14Tg2a.4 line. We also thank Drs. Yukiko Yamashita, Tomohito Higashi, William

control clones) from four independent replicates are plotted. All tested small-molecule-treated samples were statistically significant compared with controls.

(E) Quantitation of AMIS formation in GFP⁺ clones of GFP only, human MDIA1-full-length-GFP and MDIA1- Δ N3-GFP-transfected H9 cells. The average value of each independent sample (each of the three independent samples includes at least 25 individual two-cell clones) is plotted.

(F) Confocal images of H9 2-cell clones expressing human MDIA1-full-length-GFP, MDIA1- Δ N3-GFP, and GFP-only constructs stained for EZRIN are shown.

(G) hESCs were treated with graded concentrations of the ARP2/3 inhibitor, CK-666 in the presence of 10 μ M Y-27632 to prevent cell death. Quantitation of lumen formation at the two-cell stage is shown. Student's t test was performed to assess differences in lumen formation at different concentrations of all inhibitors; 2.5 μ M was used as the baseline for Y-27632 and blebbistatin in (B), while DMSO was used as the baseline for (C) and (G). The Student's t test was utilized for statistical analysis: ns = $p > 0.05$; * $p \leq 0.05$; ** $p \leq 0.01$, and *** $p \leq 0.001$. For all images, blue indicates DNA staining (DAPI). For small-molecule quantitation in (B), (C), and (G), 50 two-cell clones were counted per independent sample (total of 150 for the three samples) for each concentration. Error bars indicate SD.

(H) Proposed model for lumenogenesis in hESC and the role of RHO- and RAC-dependent actin polymerization is shown. Lumenogenesis is promoted by inhibition of ROCK-MYOSIN-II signaling (decreased contraction of the actin network), activation of MDIA1 (increased actin nucleation and extension), and activation of RAC-ARP2/3 (increased actin meshwork formation).

Scale bars represents 10 μ m in (A) and (F).



Shawlot, and Yuji Mishina for comments on the manuscript and Drs. Ann Miller, Kristen Verhey, Sivaraj Sivaramakrishnan, Ajit Joglekar, Allen Liu, and Philip Andrews for insightful discussion. PiggyBac transposon system and human MDIA1-GFP constructs were generously provided by Drs. Joseph LoTurco (CT, USA) and Shuh Narumiya (Kyoto, Japan), respectively. This work was supported by NIH grants R01-DK089933 (D.L.G.), T32-HD007505 (K.T.), F30-DK100125 (A.M.F.), R01-DK69605 (B.M.), DP2-OD-008646-01 (S.K.), R21-EB017078 (J.F.), R21-HL114011 (J.F.), and K01-DK091415 (J.R.S.), by the March of Dimes (Basil O'Connor starter scholar award) (J.R.S.), National Science Foundation (CBET1149401, J.F.), and by the Steven Schwartzberg Memorial Fund and the Prechter Fund (K.S.O.).

Received: April 6, 2015
Revised: October 26, 2015
Accepted: October 27, 2015
Published: November 25, 2015

REFERENCES

Bedzhov, I., and Zernicka-Goetz, M. (2014). Self-organizing properties of mouse pluripotent cells initiate morphogenesis upon implantation. *Cell* 156, 1032–1044.

Bryant, D.M., Roignot, J., Datta, A., Overeem, A.W., Kim, M., Yu, W., Peng, X., Eastburn, D.J., Ewald, A.J., Werb, Z., and Mostov, K.E. (2014). A molecular switch for the orientation of epithelial cell polarization. *Dev. Cell* 31, 171–187.

Burridge, K., and Wennerberg, K. (2004). Rho and Rac take center stage. *Cell* 116, 167–179.

Chan, Y.S., Göke, J., Ng, J.H., Lu, X., Gonzales, K.A., Tan, C.P., Tng, W.Q., Hong, Z.Z., Lim, Y.S., and Ng, H.H. (2013). Induction of a human pluripotent state with distinct regulatory circuitry that resembles preimplantation epiblast. *Cell Stem Cell* 13, 663–675.

Chen, H.M., DeLong, C.J., Bame, M., Rajapakse, I., Herron, T.J., McInnis, M.G., and O'Shea, K.S. (2014). Transcripts involved in calcium signaling and telencephalic neuronal fate are altered in induced pluripotent stem cells from bipolar disorder patients. *Transl. Psychiatry* 4, e375.

Gayen, S., Maclary, E., Buttigieg, E., Hinten, M., and Kalantry, S. (2015). A Primary Role for the Tsix lncRNA in Maintaining Random X-Chromosome Inactivation. *Cell Rep.* 11, 1251–1265.

Hooper, M., Hardy, K., Handyside, A., Hunter, S., and Monk, M. (1987). HPRT-deficient (Lesch-Nyhan) mouse embryos derived from germline colonization by cultured cells. *Nature* 326, 292–295.

Lancaster, M.A., and Knoblich, J.A. (2014). Organogenesis in a dish: modeling development and disease using organoid technologies. *Science* 345, 1247125.

Luckett, W.P. (1975). The development of primordial and definitive amniotic cavities in early Rhesus monkey and human embryos. *Am. J. Anat.* 144, 149–167.

Ludwig, T.E., Bergendahl, V., Levenstein, M.E., Yu, J., Probasco, M.D., and Thomson, J.A. (2006). Feeder-independent culture of human embryonic stem cells. *Nat. Methods* 3, 637–646.

Madrid, R., Aranda, J.F., Rodríguez-Fraticelli, A.E., Ventimiglia, L., Andrés-Delgado, L., Shehata, M., Fanayan, S., Shahheydari, H., Gómez, S., Jiménez, A., et al. (2010). The formin INF2 regulates basolateral-to-apical transcytosis and lumen formation in association with Cdc42 and MAL2. *Dev. Cell* 18, 814–827.

Martin-Belmonte, F., and Mostov, K. (2008). Regulation of cell polarity during epithelial morphogenesis. *Curr. Opin. Cell Biol.* 20, 227–234.

Nolen, B.J., Tomasevic, N., Russell, A., Pierce, D.W., Jia, Z., McCormick, C.D., Hartman, J., Sakowicz, R., and Pollard, T.D. (2009). Characterization of two classes of small molecule inhibitors of Arp2/3 complex. *Nature* 460, 1031–1034.

Ohgushi, M., Matsumura, M., Eiraku, M., Murakami, K., Aramaki, T., Nishiyama, A., Muguruma, K., Nakano, T., Suga, H., Ueno, M., et al. (2010). Molecular pathway and cell state responsible for dissociation-induced apoptosis in human pluripotent stem cells. *Cell Stem Cell* 7, 225–239.

Rizvi, S.A., Neidt, E.M., Cui, J., Feiger, Z., Skau, C.T., Gardel, M.L., Kozmin, S.A., and Kovar, D.R. (2009). Identification and characterization of a small molecule inhibitor of formin-mediated actin assembly. *Chem. Biol.* 16, 1158–1168.

Rodríguez-Boulan, E., and Macara, I.G. (2014). Organization and execution of the epithelial polarity programme. *Nat. Rev. Mol. Cell Biol.* 15, 225–242.

Rodríguez-Fraticelli, A.E., and Martín-Belmonte, F. (2013). Mechanical control of epithelial lumen formation. *Small GTPases* 4, 136–140.

Rossant, J., and Tam, P.P. (2009). Blastocyst lineage formation, early embryonic asymmetries and axis patterning in the mouse. *Development* 136, 701–713.

Sakamoto, S., Ishizaki, T., Okawa, K., Watanabe, S., Arakawa, T., Watanabe, N., and Narumiya, S. (2012). Liprin- α controls stress fiber formation by binding to mDia and regulating its membrane localization. *J. Cell Sci.* 125, 108–120.

Schlüter, M.A., Pfarr, C.S., Pieczynski, J., Whiteman, E.L., Hurd, T.W., Fan, S., Liu, C.J., and Margolis, B. (2009). Trafficking of Crumbs3 during cytokinesis is crucial for lumen formation. *Mol. Biol. Cell* 20, 4652–4663.

Shao, Y., Sang, J., and Fu, J. (2015). On human pluripotent stem cell control: The rise of 3D bioengineering and mechanobiology. *Biomaterials* 52, 26–43.

Straight, A.F., Cheung, A., Limouze, J., Chen, I., Westwood, N.J., Sellers, J.R., and Mitchison, T.J. (2003). Dissecting temporal and spatial control of cytokinesis with a myosin II inhibitor. *Science* 299, 1743–1747.

Tesar, P.J., Chenoweth, J.G., Brook, F.A., Davies, T.J., Evans, E.P., Mack, D.L., Gardner, R.L., and McKay, R.D. (2007). New cell lines from mouse epiblast share defining features with human embryonic stem cells. *Nature* 448, 196–199.

Wu, J., Okamura, D., Li, M., Suzuki, K., Luo, C., Ma, L., He, Y., Li, Z., Benner, C., Tamura, I., et al. (2015). An alternative pluripotent state confers interspecies chimaeric competency. *Nature* 521, 316–321.